High-Frequency Thermally Actuated Electromechanical Resonators With Piezoresistive Readout

Amir Rahafrooz, *Student Member, IEEE*, and Siavash Pourkamali, *Member, IEEE*

***Abstract*—This paper presents fabrication, characterization, and modeling of micro/nanoelectromechanical high-frequency resonators actuated using thermal forces with piezoresistive readout. Thermally actuated single-crystalline silicon resonators with frequencies (up to 61 MHz) have been successfully demonstrated. It is shown both theoretically and experimentally that, as opposed to the general perception, thermal actuation can be a viable actuation mechanism for high-frequency resonators, and using appropriate design guidelines, this actuation mechanism could even be more suitable for higher frequency rather than lower frequency applications. It has been shown through comprehensive thermoelectromechanical modeling that thermal–piezoresistive nanomechanical resonators with frequencies in the gigahertz range can exhibit motional conductance values as high as 1 mA/V while consuming static power as low as a few microwatts.**

***Index Terms*—Electromechanical modeling, high frequency, microelectromechanical system (MEMS) resonator, nanoelectromechanical system (NEMS) resonator, piezoresistive readout, thermal actuation, thermal modeling.**

I. Introduction

As the potential emerging technology for next-generation integrated frequency references, electronic filters, and resonant sensors, microelectromechanical system (MEMS) resonators have received a lot of attention over the past decade. As a result, a wide variety of high-frequency micro/nanoscale electromechanical resonators have been demonstrated lately [1]–[16]. Most of such devices use piezoelectric [1]–[3] or electrostatic (capacitive) [4]–[8] electromechanical transduction, each having its advantages and disadvantages. Piezoelectric microresonators require deposition of piezoelectric and metal thin films, generally resulting in lower quality factors and frequency and quality control issues. In the case of air-gap capacitive resonators [4]–[6], the weak electromechanical coupling leads to the need for deep-submicrometer transduction gaps, leading to fabrication challenges, power-handling limitations, and excessive squeezed-film damping when operating in air. Solid dielectric electrostatic resonator use transduction gaps filled with a solid dielectric material (preferably a high-k dielectric) to take advantage of the larger dielectric coefficients and improve the electromechanical transduction coefficients [7], [8]. The fully solid structure of such devices relaxes several problems associated with aggressive reduction of the gap sizes such as stiction and pull-in issues and allows reduction of the dielectric gap sizes to a few nanometers (as small as 15 nm demonstrated [7]). However, similar to the piezoelectric resonators, such devices require integration and physical contact of dielectric thin films and conductive electrodes with the resonator structures. This defeats some of the main purposes of moving away from piezoelectric transduction. Moreover, a large dielectric constant of the very thin dielectric films results in very large parasitic capacitors associated with such devices.

Frequency tuning and compensation of the temperature-induced frequency drift are other formidable challenges for both piezoelectric and capacitive resonators. Finally, in order to achieve strong enough electromechanical transduction, and consequently a large signal-to-noise ratio, both capacitive and piezoelectric resonators require relatively large electrode areas (thousands of micrometers), consuming costly real estate on the chip and limiting the maximum number of devices that can be integrated on a single chip.

Resonant devices combining electrostatic actuation along with active sensing mechanisms such as field effect [9] and piezoresistive [10]–[12] have been demonstrated by several researchers. This helps alleviate some of the issues associated with large motional impedances, resulting from fully electrostatic transduction. However, fabrication challenges and reliability issues associated with capacitive air gaps prevail.

Thermal actuation is a well-known mechanism that can be implemented conveniently at microscale without fabrication challenges or the need for material integration. In addition, thermal actuators have great properties such as large actuation force, low operating voltage, and simplicity of design and integration. On the downside, their relatively high power consumption usually makes them an undesirable choice. Furthermore, thermal actuators are generally considered slow actuators only suitable for dc or very low frequency applications. This is mainly due to the time delay for the temperature of a heating element to raise and generate the expected force. Consequently, although thermally actuated micromechanical resonant devices with frequencies up to 9.8 MHz have been demonstrated [13]–[17], there has not been adequate study on the possibility of utilization of thermal actuation for higher frequency applications in the very high frequency (VHF) and ultrahigh frequency

Manuscript received July 22, 2010; revised November 14, 2010 and December 18, 2010; accepted December 29, 2010. Date of publication February 22, 2011; date of current version March 23, 2011. The review of this paper was arranged by Editor A. M. Ionescu.

The authors are with the Department of Electrical and Computer Engineering, University of Denver, Denver, CO 80208 USA.

Color versions of one or more of the figures in this paper are available online at http://ieeexplore.ieee.org.

Digital Object Identifier 10.1109/TED.2011.2105491

0018-9383/$26.00 © 2011 IEEE

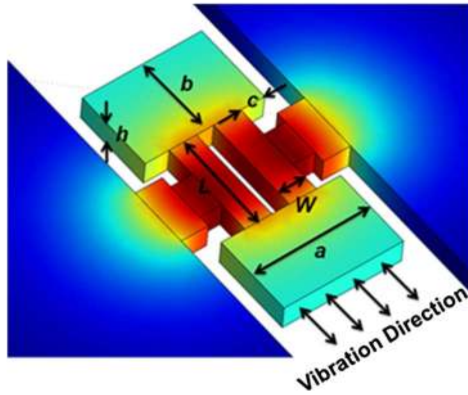

Fig. 1. Three-dimensional schematic view of a thermally actuated I^2-BAR (dog-bone resonator) showing the dimensions and the qualitative distribution of ac temperature fluctuation amplitude. (Red) Maximum. (Blue) Minimum.

(UHF) ranges. Our recent studies and experiments have shown promising results and plenty of unexplored potentials for thermally actuated high-frequency resonators [18], [19].

Both modeling and experimental measurements suggest that, as opposed to the electrostatic and piezoelectric resonators, thermal–piezoresistive resonators perform better as their size is shrunk down and, therefore, could be a much stronger candidate for realization of highly integrated nanomechanical signal processing arrays.

II. Principle of Operation and Modeling

Fig. 1 shows the schematic 3-D view of the resonator structures used in this paper, which is known as I^2-Bulk Acoustic wave Resonators or I^2-BARs [20] (also known as dog-bone resonators [11], [12]). Such structures are a great fit for thermal actuation as they can be actuated simply by applying the actuation voltage between the two support pads on their two sides. The resulting current passes through the structure heating it up by the resulting ohmic loss. The ohmic losses are maximized in the thinner parts, which are typically the extensional pillars in the middle of the structure. The fluctuating power loss results in a fluctuating temperature gradient and, therefore, periodic thermal expansion of the extensional beams. The alternating extensional force resulting from the fluctuating temperature in the pillars can actuate the resonator in its in-plane extensional resonance mode [20]. If the ohmic loss and, consequently, the resulting temperature fluctuations have the same frequency as the resonant frequency of the resonator, the mechanical vibration amplitude is amplified by the mechanical quality factor Q of the resonator. The amplified alternating stress in the pillars leads to increased fluctuations in their electrical resistance (due to the piezoresistive effect). When biased with a dc voltage, such resistance fluctuations modulate the current passing through the structure, resulting in an ac current component known as the motional current.

A. High-Frequency Thermal Actuation

It is hard to imagine a thermal system with small enough thermal time constants to respond to high-frequency excitations in the VHF and UHF ranges. Similar to electrical RC circuits, the thermal time constant of a thermal actuator (e.g., a suspended conducting beam) is the product of its thermal capacitance and thermal resistance: $\tau_{\rm th} = R_{\rm th}C_{\rm th}$. Thermal resistance can be calculated using a very similar equation to electrical resistance, i.e., $R_{\rm th} = \rho_{\rm th}L/A$, where $\rho_{\rm th}$ is the thermal resistance of the structural material, and L and A are the length and cross-sectional area of the element, respectively. Similar to electrical resistance, thermal resistance increases proportionally as the dimensions of the element are scaled down, i.e., if a thermal actuator is scaled by a factor of S, its thermal resistance changes by a factor of S^{-1}. On the other hand, thermal capacitance is proportional to the mass, and therefore to the volume of the element, and scales by a factor of S^3. Hence, the overall thermal time constant of the element scales by a factor of S^2.

On the other hand, if a mechanical structure is scaled by a factor S, its mechanical resonant frequency ω_m changes by a factor of S^{-1}, i.e., its mechanical time constant changes by a factor of S. The overall conclusion is that, if the dimensions of a thermally actuated resonant structure are scaled down, its thermal time constant shrinks more than its mechanical time constant. In other words, both thermal and mechanical responses of the system become faster upon scaling the dimensions down; however, the increase in the speed of the thermal response is more (proportional to S^{-2}) than the increase in the mechanical resonant frequency (proportional to S^{-1}). In conclusion, as the structural dimensions are scaled down, the performance of thermally actuated mechanical resonators is expected to improve (more actuation force for the same actuation power) as the thermal response of the system can better catch up with the mechanical vibrations.

Fig. 2. (a) Block-diagram demonstration of the thermoelectromechanical model of the resonator that can be divided into three subsystems of thermal, mechanical, and electrical nature. The electrical input ac voltage causes a temperature fluctuation that is turned into an ac mechanical force and, therefore, displacement. Finally, the mechanical displacement is turned into an electrical signal (motional current) due to the piezoresistive effect.

B. Thermoelectromechanical Modeling

The overall input-to-output transfer function of thermal–piezoresistive resonators includes a combination of three different domains (subsystems) of thermal, mechanical, and electrical nature, as shown in Fig. 2. First, the electrical input voltage is turned into a temperature, the temperature is then turned into a mechanical force that causes a mechanical displacement, and finally, the mechanical displacement is turned back into an electrical signal (motional current).

The first box in Fig. 2 is the thermal subsystem that turns the input voltage to a heating power (ohmic loss) and, therefore, to a temperature fluctuation amplitude $T_{\rm ac}$. Due to the square relationship between ohmic power loss and electrical voltage (or current), the application of an actuation voltage with frequency of f_a results in an ac ohmic loss component with frequency

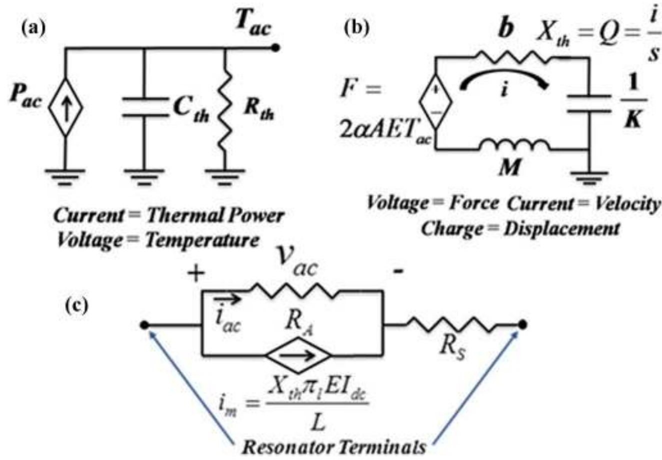

Fig. 3. (a) Equivalent electrical circuit for the thermal subsystems. (b) Equivalent electrical circuit for the mechanical subsystems. (c) Equivalent electrical circuit for the electrical subsystem.

of $2f_a$. In order to have the same frequency as the input ac actuation voltage for the thermal actuation force, a combination of ac and dc voltages (i.e., $v_{\rm ac}$ and $V_{\rm dc}$, respectively) needs to be applied between the two pads of the resonators. The resulting power loss component at the same frequency as $v_{\rm ac}$ will then be

$$P_{\rm ac} = \frac{2V_{\rm dc}v_{\rm ac}}{R_A} \tag{1}$$

where R_A is the electrical resistance of the actuator elements (extensional pillars in I^2-BARs), and $V_{\rm dc}$ and $v_{\rm ac}$ are the applied dc and ac actuation voltages, respectively.

Fig. 3(a) shows the equivalent electrical circuits of the thermal subsystem. The equivalent circuit consists of a current source representing the heating power, along with capacitance ($C_{\rm th}$) and resistance ($R_{\rm th}$) representing the effective thermal capacitance and thermal resistance of the thermal actuators, respectively. The resulting voltage across the parallel RC combination $T_{\rm ac}$ represents the temperature fluctuation amplitude, and the transfer function giving the temperature fluctuation amplitude versus the input voltage can be derived as follows:

$$H_{\rm th}(s) = \frac{T_{\rm ac}}{v_{\rm ac}} = \frac{2V_{\rm dc}R_{\rm th}}{R_A(1+R_{\rm th}C_{\rm th}s)} \tag{2}$$

where $s = j\omega$ is the Laplace transform parameter.

The alternating mechanical force amplitude due to thermal stress caused by the fluctuating temperature is

$$F = 2\alpha T_{\rm ac}AE \tag{3}$$

where α is the thermal expansion coefficient of the thermal actuator structural material, A is the thermal actuator cross-sectional area, and E is the Young's modulus of the thermal actuator along its length. The coefficient "2" has been added since there are two actuator beams in each I^2-BAR contributing to the actuation force.

In the equivalent electrical circuit of the mechanical subsystem shown in Fig. 3(b), the voltage source represents the thermally generated mechanical force, and the inductor, capacitor, and resistor represent the effective mechanical mass, stiffness, and damping of the resonator, respectively. Consequently, current represents velocity, and charge ($Q = \int I \cdot dt$) represents displacement. Therefore

$$X_{\rm th}(s) = Q(s) = \frac{i(s)}{s} = \frac{F}{(Ms^2+bs+K)} \tag{4}$$

where M, K, and b are the effective mechanical mass, spring constant, and damping coefficient of the resonant structure, and $X_{\rm th}$ is the elongation amplitude of the thermal actuators (resonator vibration amplitude). Replacing the actuation force from (3) into (4) results in the following transfer function for the mechanical subsystem:

$$H_m(s) = \frac{X_{\rm th}}{T_{\rm ac}}(s) = \frac{2\alpha AE}{(Ms^2+bs+K)}. \tag{5}$$

The undamped mechanical resonance frequency of the resonator is $\omega_0 = \sqrt{K/M}$, and its intrinsic quality factor is $Q = M\omega_0/b$. At the resonance frequency, the mechanical stiffness and mass in the mechanical transfer function cancel each other out, and H_m is simplified to

$$H_{m,\rm res} = \left.\frac{X_{\rm th}}{T_{\rm ac}}(s)\right|_{s=j\omega_0} = \frac{2\alpha AEQ}{Mj\omega_0^2} = \frac{2\alpha AEQ}{jK} \tag{6}$$

with $j = \sqrt{-1}$ showing that the mechanical displacement is lagging behind the temperature (and force) fluctuations by 90°, which is always the case for linear mechanical resonators at resonance.

The vibration amplitude, which is the output of the mechanical subsystem, causes a change in the resistivity of the thermal actuators due to the piezoresistive effect, i.e.,

$$r_{\rm ac} = R_A\pi_l E\frac{X_{\rm th}}{L} \tag{7}$$

where π_l is the longitudinal piezoresistive coefficient of the actuator beams, $r_{\rm ac}$ is the amplitude of the actuator resistance fluctuations, and L is the length of the thermal actuators. Since a dc bias voltage is applied to the thermal actuators, this change in resistance modulates the current in the actuators, i.e.,

$$i_m = \frac{r_{\rm ac}}{R_A}I_{\rm dc}. \tag{8}$$

Therefore, the transfer function of the electrical subsystem [see Fig. 3(c)] will be as follows:

$$H_e = \frac{i_m}{X_{\rm th}} = \frac{\pi_l EI_{\rm dc}}{L}. \tag{9}$$

R_s in Fig. 3(c) represents all the parasitic electrical resistances in series with the actuator resistance, which mainly includes resistance of resonator support beams.

Finally, the overall transfer function that relates the ac motional current (output current) to the ac input voltage is the product of the three transfer functions of the thermal, mechanical, and electrical subsystems, i.e.,

$$H_T = \frac{i_m}{v_{\rm ac}} = H_{\rm th} H_m H_e = \frac{4\alpha A E^2 I_{\rm dc}^2 \pi_l}{L(Ms^2+bs+K)} \frac{R_{\rm th}}{(1+R_{\rm th}C_{\rm th}s)} \tag{10}$$

which simplifies as following at resonance frequency:

$$H_T|_{s=j\omega_0} = \frac{4\alpha E^2 \pi_l Q A I_{\rm dc}^2}{KLj} \frac{R_{\rm th}}{(1+R_{\rm th}C_{\rm th}s)}. \tag{11}$$

Furthermore, for physical dimensions in the microscale and even nanoscale, the thermal time constant is typically much larger than the mechanical time constant of the structure. In other words, it takes a much longer than the mechanical resonance period of the structure for the temperature of the actuators to reach its steady-state value and stabilize. Therefore, $\omega_0 \gg \tau_{\rm th}^{-1} = (R_{\rm th}C_{\rm th})^{-1}$, which simplifies H_T to

$$H_T|_{s=j\omega_0} = g_m = 4\alpha E^2 \pi_l Q \frac{A I_{\rm dc}^2}{K L C_{\rm th}\omega_0}. \tag{12}$$

Knowing that $K = 2EA/L$, (12) can be further simplified to

$$g_m = 2\alpha E \pi_l Q \frac{I_{\rm dc}^2}{C_{\rm th}\omega_0}. \tag{13}$$

The transfer function in (12) and (13) can be referred to as small signal voltage to current gain, or motional conductance g_m of the resonator at its resonance frequency, which is one of the most important parameters of a thermal–piezoresistive resonator when utilized as an electronic circuit component.

C. Resonator Equivalent Electrical Circuit

For the single-port I^2-BAR resonators used in this paper, where the resonator extensional pillars acting as thermal actuators also act as piezoresistive sensors, the physical resistance of the resonator connects the input and output of the devices. Therefore, the equivalent electrical circuit includes a resistance $R_A + R_s$ connected between the two terminals of the resonator, which is the overall resistance in the current path between the two pads of the resonator. In parallel to the static resistance of the actuators, there is a series RLC combination that represents the mechanical resonant behavior of the structure. The value of R_m in the RLC has to be set so that, at resonance, a motional current of $i_m = g_m \cdot v_{\rm ac} = v_{\rm ac}/R_m$ is added to the feedthrough current passing through R_A. Therefore, $R_m = g_m^{-1}$ and L_m and C_m values can be calculated based on the value of R_m, as shown in Fig. 4, according to the resonance frequency and quality factor of the resonator.

D. Calculation of Actuator Thermal Capacitance

To calculate the g_m of a thermal–piezoresistive I^2-BAR, which is the most important parameter to be extracted from the model, using (12), all the parameters except the effective thermal capacitance of the actuators $C_{\rm th}$ are known for every set of resonator dimensions. Due to the distributed nature of the thermal parameters, including the thermal generator (resistance of the structure), thermal capacitance, and thermal conductance, analytical derivation of the effective equivalent values for the thermal parameters could be quite complicated. Therefore, COMSOL finite-element analysis was used to analyze the ac thermal behavior of the actuators and calculate the fluctuating temperature amplitude $T_{\rm ac}$ at different points along the length of the actuator beams (Fig. 5). The mean value of the small signal temperature amplitudes at different points along the actuators is the effective temperature fluctuation amplitude for the actuator.

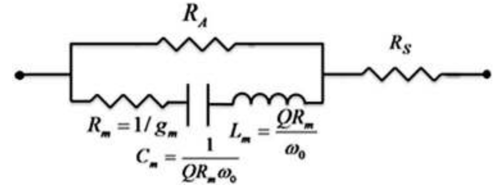

Fig. 4. Overall equivalent electrical circuit for one-port thermally actuated resonators with piezoresistive readout.

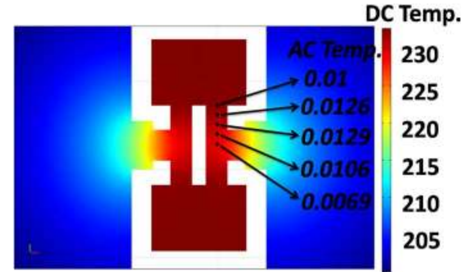

Fig. 5. COMSOL finite-element thermal analysis of a 61-MHz I^2-BAR by applying dc and ac currents of 60 and 5 mA, respectively. The color code shows static temperature of the structure resulting from the dc bias current, and the numbers show temperature fluctuation amplitude $T_{\rm ac}$ at different points along the actuator caused by the ac excitation, showing temperature fluctuation amplitude of $\sim$0.01 °C at a point in the middle of the thermal actuator.

Again, using the typically valid assumption of $\omega \gg \tau_{\rm th}^{-1} = (R_{\rm th}C_{\rm th})^{-1}$, $C_{\rm th}$ can be calculated using the value of $T_{\rm ac}$ obtained from the finite-element analysis and a rearranged and simplified version of (2), i.e.,

$$C_{\rm th} = \frac{2 I_{\rm dc} i_{\rm ac} R_A}{T_{\rm ac}\omega_m}. \tag{14}$$

E. Resonator Scaling Behavior

Looking at the scaling behavior of g_m as the resonator dimensions are scaled down, the following proportionalities can be identified: $A \propto S^2$, $C_{\rm th} \propto S^3$, $L \propto S$, $K \propto S$, and $\omega_0 \propto S^{-1}$, where S is the scaling factor. Consequently, assuming the same resonator quality factor and bias current, $g_m \propto s^{-2}$, i.e., g_m increases with a square relationship as the resonator is scaled down, whereas at the same time, the resonator resonant frequency is increasing proportionally. This further confirms the explanation provided previously justifying the suitability of thermal actuation for high-frequency applications.

The alternative way of looking at this is that the same g_m values as the low-frequency resonators can be achieved for

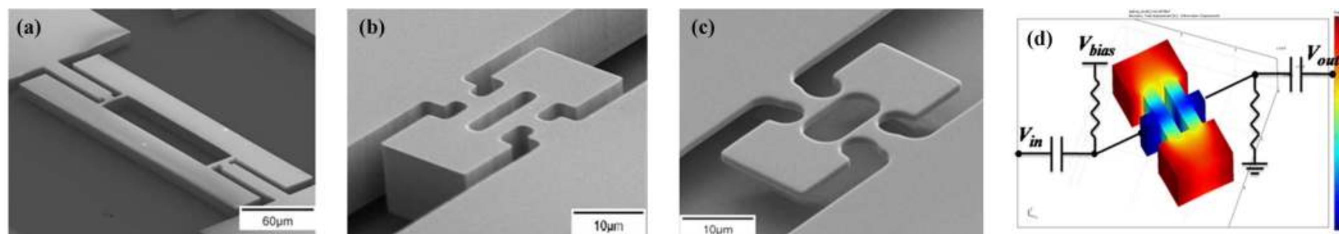

Fig. 6. (a) SEM view of a 7.9-MHz 15-μm-thick I^2-BAR fabricated on a low-resistivity p-type substrate. (b) SEM view of a 61-MHz 15-μm-thick I^2-BAR fabricated on a low-resistivity p-type substrate. (c) SEM view of a 41-MHz 3-μm-thick I^2-BAR fabricated on a low-resistivity n-type substrate followed by thermal oxidation to thin down its thermal actuator beams. All devices are fabricated on 100 SOI substrates. The first two resonators are oriented along the 110 crystalline orientation, whereas the third resonator is aligned to the 100 crystalline orientation; (d) Schematic of the electrical connections for operation of an I^2-BAR in a one-port configuration along with the COMSOL modal analysis results, showing the in-plane fundamental extensional resonance mode for the resonator of Fig. 6(b). The resonator dimensions are $a = 22$ μm, $b = 15$ μm, $c = 4.4$ μm, $L = 18$ μm, and $W = 5$ μm, showing a frequency of 60.77 MHz. Red and blue colors show locations with the largest and smallest vibration amplitudes, respectively.

higher frequency devices while having proportionally less bias current. This means proportionally less power consumption, assuming the same electrical resistivity for the resonator structural material.

III. Resonator Fabrication and Measurement

A single-mask process was used to fabricate the resonators on low-resistivity silicon-on-insulator (SOI) substrates [19]. The fabrication process starts by thermally growing a thin (∼200 nm) layer of silicon dioxide on the device layer that will serve as a hard mask for silicon etching. The silicon dioxide layer is patterned to define the resonator structures. The structures are then carved into the SOI device layer all the way down to the buffer oxide (BOX) layer by plasma etching. Finally, the structures are released by etching the underlying BOX layer in hydrofluoric acid (HF). At the same time, the remaining oxide mask on top of the structures is also etched away.

A wide variety of I^2-BAR structures with different dimensions were fabricated on SOI substrates with different device layer thickness, resistivity, and doping type. Fig. 6 shows the scanning electron microscopy (SEM) view of a few of the fabricated resonators. For some of the devices, the actuator beams were thinned down in order to minimize resonator power consumption. By performing a number of consecutive thermal oxidation and oxide removal steps, submicrometer actuator widths were achieved [see Fig. 6(c)].

Since the resonant structures in this paper are one-port devices composed of a monolithic piece of crystalline silicon, they were tested in a one-port configuration. In a one-port configuration, the extensional beams act simultaneously as both thermal actuators and piezo-resistive sensors. Fig. 6(d) shows the schematic of the electrical connections required for operation of the resonator in the one-port configuration along with COMSOL modal analysis results for the 61-MHz resonator shown in Fig. 6(b) in its fundamental in-plane extensional mode. In this configuration, a combination of a dc bias current and an ac actuation voltage are applied between the two terminals of the resonator. Large bypass capacitors and bias resistors are used to isolate the ac and dc sources.

Due to the very low resistance of the actuator beams on the order of a few ohms, only a small portion of the applied

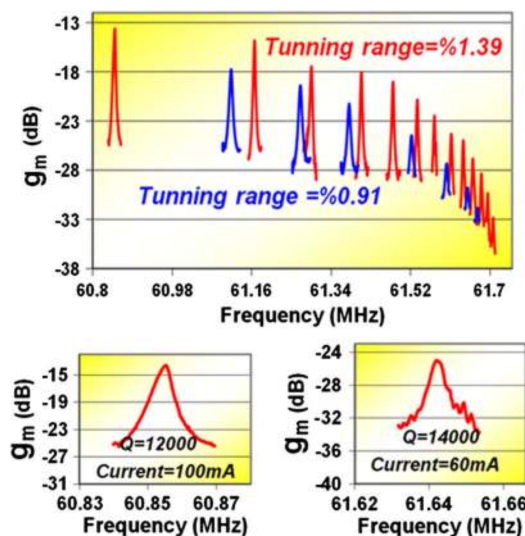

Fig. 7. Measured frequency response of the thermally actuated 61-MHz resonator of Fig. 6(b) with different bias currents. The vertical axis in the frequency response plots shows the motional transconductance of the resonators g_m in dB. Red and blue plots refer to vacuum and air testing conditions, respectively. Current range is 45–100 mA in vacuum and 55–100 mA in air.

voltage by the network analyzer through its 50-Ω terminations will fall across the actuators, resulting in excessive attenuation in the transmission spectra. Therefore, the effect of the bias resistors, the 50-Ω terminations of the network analyzer, and the parasitic resistances associated with the resonator structures should be deembedded from the measured data before comparing them with the theoretically calculated values [21]. Fig. 7 shows motional conductance values after deembedding the effect of parasitic and bias resistors from data obtained from the 61-MHz resonator in Fig. 6(b). For this resonator, quality factors ranging from 12 000 to 14 000 were measured under vacuum. The quality factor dropped to 6000 to 8000 under atmospheric pressure. A large-frequency tuning range can be achieved for such resonators by changing their dc bias currents. This is mainly due to the raising temperature of the resonating body, particularly its extensional beams that provide most of the structural stiffness in the in-plane extensional mode. As expected, as the dc bias current increases, the output signal level increases, whereas due to the higher static temperature and softening of the structural material, the resonant frequency decreases.

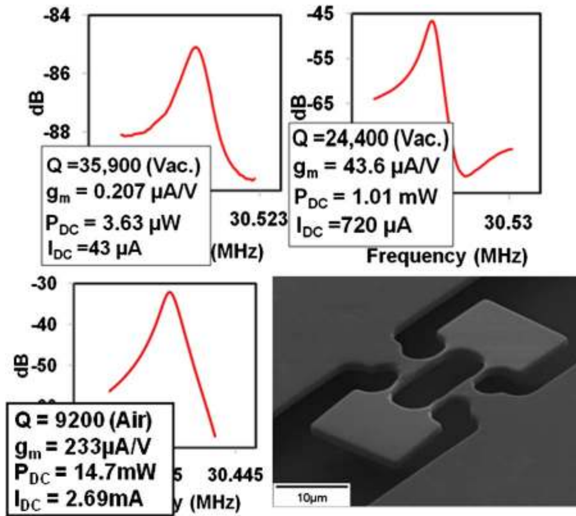

Fig. 8. SEM view and measurement results for a 3-μm-thick 30.5-MHz dog-bone resonator. The vertical axis in the frequency response plots shows the motional transconductance of the resonators g_m in decibels. Due to its very narrow (750-nm-wide) actuator beams, clear resonant peaks with motional conductance in the tens of microamperes per volt have been measured for this resonator with submilliampere dc bias currents (submilliwatt power consumption).

It should be noted that, according to Fig. 4, in one-port measurements, signal transmission through the resonator includes the feedthrough signal through the electrical resistance of the structure $(R_A + R_S)$. The frequency responses shown in Fig. 7 and other upcoming frequency response plots only include the motional current passing through the structure obtained by elimination of the feedthrough signal from the overall measured current passing through the resonator.

Although operating at high frequencies, unprecedented for thermally actuated resonators, and with high quality factors, the large current requirement and power consumption for the resonator in Fig. 7 is a major drawback against using such as electronic components. Therefore, for a number of fabricated resonators, the actuator widths were reduced by oxidizing them in order to consume a thin layer of silicon on their surfaces, including on their actuator beams. After removal of the grown oxide layer, a thinner extensional beam is left. This sequence was repeated a few times for some of the resonators until submicrometer beamwidths were achieved.

Fig. 8 shows some of the frequency responses measured for one of such devices with a resonant frequency of 30.5 MHz and $\sim$750-nm-wide actuators. As opposed to the 61-MHz resonator of Fig. 7 that required at least 40 mA of dc bias to exhibit a measurable resonance peak, a resonance peak was detected for this resonator with currents as low as 43 μA translating into dc power consumption values as low as 3.6 μW. At the dc bias current of 720 μA (dc power of 1 mW), motional conductance of 44 μA/V was measured for this resonator. Maximum currents tolerable for such narrow actuator beams are in the few milliampere range, leading to motional conductance values as high as 0.23 mA/V in air with Q of 9200. According to the derived model, much higher motional conductance values can be achieved by consuming the same amount of power using lower resistivity structural materials, allowing higher bias

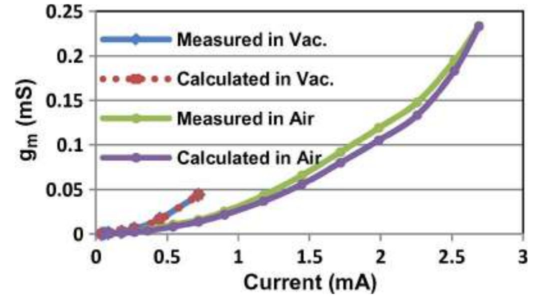

Fig. 9. Measured and calculated values of motional conductance versus bias current in both air and vacuum for the 30.5-MHz resonator shown in Fig. 8, showing an acceptable agreement between the recordings and the model predictions. Measured Q values are used to find the calculated values.

currents. This resonator was fabricated on an N-type SOI device layer with resistivity of $\sim 0.02\ \Omega \cdot \text{cm}$. Therefore, another one to two orders of magnitude improvement are expected to be achievable using lower resistivity substrates. Fig. 9 shows a comparison between the measured and calculated motional conductance values in both air and vacuum for the 30.5-MHz resonator of Fig. 8.

In order to examine and verify the validity of the derived model, several measurement results for I^2-BAR resonators with different dimensions were compared with the values calculated by the model. Table I presents some of the measured data for different resonators under different bias current and pressure conditions. Considering the several possible sources of error, there is a good agreement between the measured and calculated g_m values for most of the data points. Some of the major sources of error include uncertainty in resistivity and other physical properties of the structural material (e.g., piezoresistive coefficient), as well as changes in such properties at elevated temperatures, uncertainty in structural dimensions and rounded corners and concave shape of the actuator beams (particularly for smaller devices), and errors in extraction of the motional conductance values from the logarithmic measured transmission data (from the network analyzer) and deembedding the effect of the parasitic resistances.

IV. Resonator Optimization and Behavior Prediction

In order to achieve higher performance for the thermal–piezoresistive resonators, it is desirable to maximize the resonator motional conductance g_m (for an improved signal-to-noise ratio) with minimal power consumption. Therefore, a figure of merit for the resonators has been defined as the ratio of the resonator g_m to the overall dc power consumption, i.e.,

$$\text{F.M.} = \frac{g_m}{P_{\text{dc}}} = \frac{2\alpha E \pi_l Q}{C_{\text{th}} \omega_0 (R_A + R_s)} \tag{15}$$

where $P_{\text{dc}} = I_{dc}^2 \cdot (R_A + R_S)$ is the dc power consumption of the resonator. The different parameters that can be used to maximize F.M. are given in the following sections.

TABLE I
MEASUREMENT AND CALCULATION RESULTS FOR DIFFERENT THERMAL–PIEZORESISTIVE I²-BARS

Scale Factor	Resonator Dimensions (μm)						Measured Parameters				Calculated Parameters					
	a	b	c	L	W	H(μm) Resistivity (Ω.cm)	Current (mA)	Q. Factor	Freq. (MHz)	g_m (mA/V)	Power (mW)	R_A (Ω)	C_{th} (nJ/°K)	g_m (mA/V)	F.M./Q. (10^{-6} V^{-2})	Power (mW) @ g_m=1 (mA/V)
1X	274	30	67	31	4	10 1.5×10^{-3}	16.8	29000	7.94	2.53	6.00	5.81	2.02	2.93	16.8	2.05
							40.5	37000	7.75	27.0	34.9			23.3	18.1	1.49
0.7X	193	21	47	22	2.7		26	24000	10.87	10.2	16.3	6.11	0.968	9.12	23.2	1.79
							30.5	16000	10.63	10.9	22.5			8.95	24.8	2.52
0.5X	144	16	35	16	2		21.3	12000	13.94	5.80	10.8	6.00	0.521	4.83	37.0	2.25
							30.2	7000	13.78	10.0	21.8			5.86	38.3	3.73
1X	80	53	16	64	17.4	10 6×10^{-3}	55	28500	15.89	2.18	63.5	11.0	18.1	1.56	0.86	40.6
							80	29000	15.65	8.08	134			3.52	0.90	38.2
							50	10800	15.91	0.60	52.5			0.49	0.86	107
							90	10900	15.73	4.29	170			1.65	0.89	103
0.5X	39	25	8.5	32	8.5		20	29000	31.18	0.319	9.09	11.3	4.43	0.48	1.82	18.9
							65	38500	30.72	11.3	96.0			7.04	1.90	13.6
							30	11000	31.17	0.271	20.4			0.41	1.82	49.8
							70	12000	30.9	2.88	111			2.50	1.87	44.5
NA	18.5	11.5	4.4	14.9	0.77	3 2×10^{-2}	0.043	36000	30.52	2.07×10^{-4}	1.71×10^{-3}	645	5.61×10^{-2}	2.30×10^{-4}	3.73	7.44
							0.72	24400	30.52	4.36×10^{-2}	0.481			4.38×10^{-2}	3.73	10.9
							0.062	13250	30.52	1.42×10^{-4}	3.56×10^{-3}			1.76×10^{-4}	3.73	20.2
							2.69	9200	30.43	0.234	6.71			0.233	3.77	28.8
NA	18.5	12.3	4.4	12.9	1.03		0.544	3800	41.73	4.87×10^{-4}	0.220	417	6.50×10^{-2}	1.06×10^{-3}	1.26	208
							5.32	2600	40.60	1.98×10^{-2}	21.1			7.51×10^{-2}	1.37	280
							0.363	2700	40.60	2.32×10^{-4}	0.098			3.63×10^{-4}	1.37	270
							5.21	2300	40.70	3.37×10^{-2}	20.3			6.34×10^{-2}	1.36	319
NA	12.9	9	3	8.67	0.43		0.441	1400	45.20	8.88×10^{-4}	0.182	672	1.82×10^{-2}	8.87×10^{-4}	3.49	204
							5.55	1700	43.78	5.28×10^{-2}	28.8			0.188	3.84	153
							0.266	1300	45.20	3.72×10^{-4}	0.066			3.00×10^{-4}	3.49	220
							5.47	1500	43.90	6.33×10^{-2}	28.0			0.160	3.81	175
NA	22	15	4.4	18	5	15 3.5×10^{-3}	60	14000	61.64	5.73	32.3	4.20	2.20	5.4	11.8	6.01
							100	12000	60.85	21.5	89.8			15.7	14.5	5.73
							60	7500	61.65	3.38	32.3			3.39	13.9	9.53
							100	7700	61.11	12.9	89.8			9.9	14.3	9.04
	= data obtained under atmospheric pressure															

A. Actuator Beam Dimensions

Generally, smaller actuator dimensions lead to smaller C_{th}, improving the resonator figure of merit. However, the effect of actuator dimensions on its electrical resistance R_A should also be taken into account.

Since the extensional stiffness of the actuator beams define the I²-BAR resonant frequency, in order to maintain the same resonant frequency for an I²-BAR while reducing its actuator thermal capacitance, both length and width of the actuator should be scaled down simultaneously. Such scaling does not affect the actuator electrical resistance R_A. Therefore, scaling down both the length and width of the actuator beams by a scale S_a results in an improvement in the resonator F.M. by a factor of S_a^2 while maintaining an almost constant resonant frequency for the device.

B. Resonant Frequency and Resonator Scaling

At a first glance at (15), higher frequencies seem to have a deteriorating effect on the resonator figure of merit. However, if higher resonant frequencies are achieved by shrinking the resonator size at the same time, C_{th} will be shrinking sharply.

If all resonator dimensions are scaled down proportionally by a factor S, $C_{\text{th}} \propto S^{-3}$, $\omega_0 \propto S$, and $(R_A + R_S) \propto S$. Therefore, F.M. $\propto S$, i.e., F.M. increases proportionally if the resonator dimensions are scaled, increasing its resonant frequency at the same time.

To experimentally investigate the effect of resonator scaling, scaled versions of similar resonators (with the same horizontal dimensional aspect ratios) were included in the layout and fabricated. In order to have a fair comparison between F.M. values for different resonators, the effect of resonator mechanical quality factor was factored out by defining a coefficient K, which is defined as

$$K = \frac{\text{F.M.}}{Q}. \tag{16}$$

Values of K coefficients extracted from the measurement results for different resonators under different dc bias current are shown in Fig. 10, with the data corresponding to similar resonators with different scales presented on the same axes.

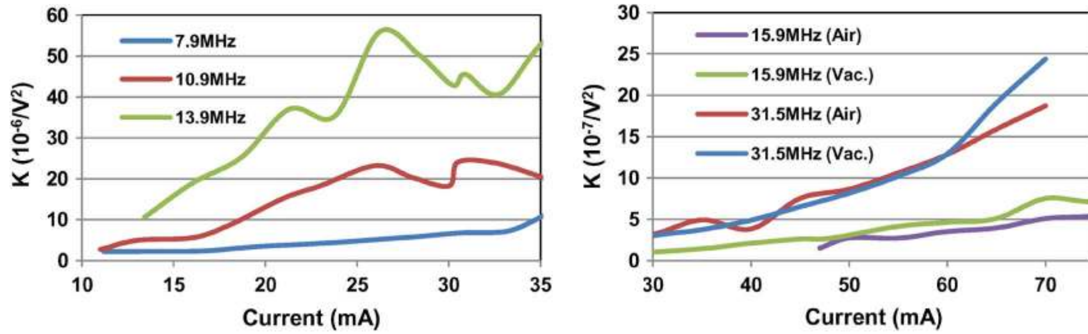

Fig. 10. Extracted K values for similar scaled resonators versus resonator bias current. In both sets of resonators, the smaller (higher frequency) devices have higher transduction strength.

TABLE II
PREDICTED RESONATOR PERFORMANCE PARAMETERS FOR TWO SCALED-DOWN VERSIONS OF THE 61-MHz RESONATOR OF FIG. 7 WITH RESONANT FREQUENCIES OF 900 MHz AND 2.1 GHz OBTAINED FROM THE DEVELOPED MODEL

Scale Factor	Resonator Dimensions (µm)						Measured/Assumed Parameters			Calculated Parameters				
	a	*b*	*c*	*L*	*W*	*h*	Current (mA)	Q. Factor	Freq. (MHz)	Power (mW)	R_A (Ω)	g_m (mA/V)	F.M. ($10^{-6}/V^2$)	Power (µW) @ g_m=1 (mA/V)
1X	22	15	4.4	18	5	15	60	14000	61.64	32.3	4.2	5.4	11.8	6013
0.0723X				1.3	0.36		4.67	14000	900	2.40	58.5	5.4	161	445
0.5X Act.*	1.59	1.08	0.39	0.65	0.18	1.08	2.24	14000	904.5	0.578	58.5	5.4	667	107
0.25X Act.*				0.32	0.09		1.09	14000	905.7	0.139	57.6	5.4	2775	25.7
0.031X				0.56	0.15		1.99	14000	2100	1.02	142	5.4	378	189
0.5X Act.*	0.68	0.46	0.14	0.28	0.075	0.46	0.961	14000	2111	0.246	142	5.4	1567	45.6
0.25X Act.*				0.14	0.037		0.475	14000	2113	6.18×10^{-2}	143	5.4	6243	11.4

* Scale factors identified by "Act*" show devices for which actuator sizes have been further scaled down in addition to the overall scaling of the resonator.

These plots confirm that smaller scale resonators with higher resonance frequencies have higher transduction strength.

It can be concluded from the last two discussions that the capability to fabricate resonator actuator beams with very small (nanoscale) dimensions is the key to achieving very high performance levels for thermal–piezoresistive I^2-BARs, both at low and high frequencies.

C. Electrical Resistivity and Other Material Properties

The most important parameter that can also be controlled for some of the most popular resonator structural materials (e.g., Si or SiC) is the electrical resistivity of the structural material. Lower electrical resistivity of the structural material improves the resonator transduction figure of merit by lowering $R_A + R_s$. This can be explained by the fact that, with lower electrical resistivity, the same amount of dc bias current, and therefore the same motional conductance, can be maintained while burning less ohmic power in the structure. A number of other structural material properties also affect the figure of merit for the thermal–piezoresistive resonators. Higher thermal expansion coefficient and lower specific heat capacity improve thermal actuation, resulting in proportionally higher F.M.. Higher piezoresistive coefficient improves the piezoresistive readout having the same effect on F.M.. One interesting and promising fact is the giant piezoresistive effect found in single-crystalline silicon nanowires that has been observed and reported by different researchers [22]. Therefore, as the resonators are scaled down to reach higher resonant frequencies in the hundreds of megahertz and gigahertz range, it is expected that the actuator beams with deep-submicrometer width exhibit such strong piezoresistivity, significantly improving resonator performances.

Using structural materials with higher Young's modulus E can also improve the resonator figure of merit while increasing its resonant frequency.

D. Thermal Actuation at Gigahertz Frequencies

It was shown through theoretical derivations and measurements that thermal actuation is not only a suitable mechanism for high-frequency resonator applications, but also it can provide higher performances at higher rather than lower frequencies. Here, the derived resonator model is utilized to predict the performance of higher frequency thermal–piezoresistive I^2-BARs with resonant frequencies in the gigahertz range. Two scaled-down versions of the 61-MHz resonator of Fig. 6(b) with resonant frequencies of 900 MHz and 2.1 GHz with resistivity of $3.5 \times 10^{-3}\ \Omega \cdot$ cm were analyzed using the developed model. The results are presented in Table II, showing that g_m as high as 1 mA/V can be achieved for such high-frequency resonators with power consumption values in the submilliwatt range. The

same g_m values with much lower power consumption can be achieved on lower resistivity substrates. Table II also includes calculated characteristics for resonators with scaled-down actuator dimensions to further minimize their power consumption values (maximize F.M.). For such devices, power consumption as low as a few microwatts can provide motional conductance of 1 mA/V.

It should be noted that, for all the calculations presented in Table II, the bulk piezoresistive coefficient of silicon has been used. However, for such high-frequency resonators, thermal actuators are practically silicon nanowires and are expected to have up to 40× higher piezoresistive coefficients than that of bulk silicon [22]. Therefore, it is expected that the resonator performances in the gigahertz range will even be better than what is shown in Table II.

V. Conclusions and Future Work

Thermally actuated high-frequency single-crystalline silicon resonators with frequencies up to 61 MHz have been successfully fabricated and characterized. It was shown through electrothermomechanical modeling and measurements that, as opposed to the general perception, thermal actuation is a viable and potentially very suitable transduction mechanism for high-frequency applications.

The derived resonator model was validated using the experimental data obtained from different resonators, showing a good agreement between the measurements and model predictions. The effect of several design parameters and material properties on the performance of the resonators was discussed, providing guidelines for improved designs. The modeling strategy developed here can be applied to a wide variety of thermally actuated micromechanical resonators with slight modifications. Based on the analysis in this paper, unlike electrostatic or piezoelectric transducers that require large electrode area, thermal–piezoresistive transduction exhibits improved performance as the resonator structural features are scaled down into nanoscale.

Therefore, it could be the only suitable transduction mechanism for next-generation highly integrated nanomechanical resonator arrays. It was shown that thermal actuation of nanoscale resonators with frequencies in the gigahertz range is theoretically feasible and the power consumption for such devices can be as low as a few microwatts.

Future work includes further design optimization and miniaturization of the resonator dimensions to achieve better resonator performance and higher frequencies. Using other resonator topologies and multilayer two port configurations as well as examination of other structural materials are among other future directions.

References

[1] M. Rinaldi, C. Zuniga, C. Zuo, and G. Piazza, "Super-high-frequency two-port AlN contour-mode resonators for RF applications," *IEEE Trans. Ultrason., Ferroelectr., Freq. Control*, vol. 57, no. 1, pp. 38–45, Jan. 2010.

[2] G. K. Ho, R. Abdolvand, A. Sivapurapu, S. Humad, and F. Ayazi, "Piezoelectric-on-silicon lateral bulk acoustic wave micromechanical resonators," *J. Microelectromech. Syst.*, vol. 17, no. 2, pp. 512–520, Apr. 2008.

[3] A. Artieda and P. Muralt, "High- Q AlN/ SiO_2 symmetric composite thin film bulk acoustic wave resonators," *IEEE Trans. Ultrason., Ferroelectr., Freq. Control*, vol. 55, no. 11, pp. 2463–2468, Nov. 2008.

[4] C. T. C. Nguyen, "MEMS technology for timing and frequency control," *IEEE Trans. Ultrason., Ferroelectr., Freq. Control*, vol. 54, no. 2, pp. 251–270, Feb. 2007.

[5] S. Pourkamali, G. K. Ho, and F. Ayazi, "Low-impedance VHF and UHF capacitive silicon bulk acoustic wave resonators," *IEEE Trans. Electron Devices*, vol. 54, no. 8, pp. 2017–2023, Aug. 2007.

[6] S. Pourkamali, Z. Hao, and F. Ayazi, "VHF single crystal silicon side supported disk resonators—Part II: Implementation and characterization," *J. Microelectromech. Syst.*, vol. 13, no. 6, pp. 1054–1062, Dec. 2004.

[7] D. Weinstein and S. A. Bhave, "Internal dielectric transduction of a 4.5 GHz silicon bar resonator," in *IEDM Tech. Dig.*, Washington, DC, Dec. 2007, pp. 415–418.

[8] S. A. Bhave and R. T. Howe, "Silicon nitride-on-silicon bar resonator using internal electrostatic transduction," in *Proc. 13th Int. Conf. Solid-State Sens., Actuators, Microsyst. (Transducers)*, Seoul, Korea, Jun. 2005, vol. 2, pp. 2139–2142.

[9] D. Grogg, M. Mazza, D. Tsamados, and A. M. Ionescu, "Multi-gate vibrating-body field effect transistor (VB-FETs)," in *IEDM Tech. Dig.*, San Francisco, CA, Jun. 2008, pp. 663–666.

[10] J. T. M. van Beek, G. J. A. M. Verheijden, G. E. J. Koops, K. L. Phan, C. van der Avoort, J. van Wingerden, D. Ernur Badaroglu, and J. J. M. Bontemps, "Scalable 1.1 GHz fundamental mode piezo-resistive silicon MEMS resonator," in *IEDM Tech. Dig.*, Washington, DC, Dec. 2007, pp. 411–414.

[11] J. T. M. van Beek, K. L. Phan, G. J. A. M. Verheijden, G. E. J. Koops, C. van der Avoort, J. van Wingerden, D. Ernur Badaroglu, J. J. M. Bontemps, and R. Puers, "A piezo-resistive resonant MEMS amplifier," in *IEDM Tech. Dig.*, San Francisco, CA, Jun. 2008, pp. 667–670.

[12] J. J. M. Bontemps, A. Murroni, J. T. M. van Beek, J. A. T. M. van den Homberg, J. J. Koning, G. E. J. Koops, G. J. A. M. Verheijden, J. van Wingerden, K. L. Phan, P. Vermeeren, C. van der Avoort, H. C. W. Beijerinck, and P. G. M. Baltus, "56 MHZ piezoresistive micromechanical oscillator," in *Proc. 16th Int. Conf. Solid-State Sens., Actuators, Microsyst. (Transducers)*, Denver, CO, Jun. 2009, pp. 1433–1436.

[13] R. J. Wilfinger, P. H. Bardell, and D. S. Chhabra, "The resonistor: A frequency selective device utilizing the mechanical resonance of a silicon substrate," *IBM J. Res. Develop.*, vol. 12, no. 1, pp. 113–118, Jan. 1968.

[14] R. B. Reichenbach, M. Zalalutdinov, J. M. Parpia, and H. G. Craighead, "RF MEMS oscillator with integrated resistive transduction," *IEEE Electron Device Lett.*, vol. 27, no. 10, pp. 805–807, Oct. 2006.

[15] K. L. Phan, P. G. Steeneken, M. J. Goossens, G. E. J. Koops, G. J. A. M. Verheijden, and J. T. M. van Beek, Spontaneous Mechanical Oscillation of a DC Driven Single Crystal, 2009, ArXiv 0904.3748.

[16] J. H. Seo and O. Brand, "High Q-factor in-plane-mode resonant microsensor platform for gaseous/liquid environment," *J. Microelectromech. Syst.*, vol. 17, no. 2, pp. 483–493, Apr. 2008.

[17] A. Hajjam, A. Rahafrooz, J. C. Wilson, and S. Pourkamali, "Thermally actuated MEMS resonant sensors for mass measurement of micro/nanoscale aerosol particles," in *Proc. 8th IEEE Sensors*, Christchurch, New Zealand, Oct. 2009, pp. 707–710.

[18] A. Rahafrooz and S. Pourkamali, "Thermo-electro-mechanical modeling of high frequency thermally actuated I^2-BAR resonators," in *Proc. Tech. Dig. Solid-State Sens., Actuator, Microsyst. Workshop*, Hilton Head Island, SC, Jun. 2010, pp. 74–77.

[19] A. Rahafrooz, A. Hajjam, B. Tousifar, and S. Pourkamali, "Thermal actuation, a suitable mechanism for high-frequency electromechanical resonators," in *Proc. 23rd IEEE MEMS*, Hong Kong, Jan. 2010, pp. 200–203.

[20] G. K. Ho, K. Sundaresan, S. Pourkamali, and F. Ayazi, "Micromechanical IBARs: Tunable high- Q resonators for temperature-compensated reference oscillators," *J. Microelectromech. Syst.*, vol. 19, no. 3, pp. 503–515, Jun. 2010.

[21] A. Hajjam, J. C. Wilson, A. Rahafrooz, and S. Pourkamali, "Fabrication and characterization of thermally actuated micromechanical resonators for airborne particle mass sensing, Part II: Device fabrication and characterization," *J. Micromech. Microeng. (JMM)*, vol. 20, no. 12, p. 125 019, Dec. 2010.

[22] R. He and P. Yang, "Giant piezoresistance effect in silicon nanowires," *Nat. Nanotechnol.*, vol. 1, no. 1, pp. 42–46, Oct. 2006.

Amir Rahafrooz (S'07) received the B.Sc. degree in biomedical engineering from Isfahan University, Isfahan, Iran, in 2004, and the M.Sc. degree in bioelectrics from Amirkabir University of Technology, Tehran, Iran, in 2007. He is currently working toward the Ph.D. degree in the Department of Electrical and Computer Engineering, University of Denver, Denver, CO.

His research interests are mainly related to microelectromechanical system frequency references and resonant sensors.

Mr. Rahafrooz was the recipient of the 2009 University of Denver School of Engineering and Computer Science Best Research Assistant Award. He is also the recipient of the 2009–2010 University of Denver Graduate Studies Fellowship for Inclusive Excellence.

Siavash Pourkamali (S'02–M'06) received the B.S. degree in electrical engineering from Sharif University of Technology, Tehran, Iran, in 2001 and the M.S. and Ph.D. degrees in electrical engineering from Georgia Institute of Technology (Georgia Tech), Atlanta, in 2004 and 2006, respectively.

He is currently an Assistant Professor with the Department of Electrical and Computer Engineering, University of Denver, Denver, CO. He is the holder of several patents in the areas of silicon micro/nanomechanical resonators and filters and nanofabrication technologies. His main research interests are in the areas of integrated silicon-based microelectromechanical systems (MEMS), micromachining technologies, radio frequency MEMS resonators and filters, and nanomechanical resonant sensors.

Dr. Pourkamali was the recipient of a Silver Medal in the 1997 International Chemistry Olympiad, the 2005 Georgia Tech Sigma Xi Best M.S. Thesis Award, the 2006 Georgia Tech Electrical and Computer Engineering Research Excellence Award, the 2008 University of Denver Best Junior Scholar Award, and the 2011 National Science Foundation CAREER Award.